

Power Laws Dominate Shear and Extensional Rheology Response and Capillarity-Driven Pinching Dynamics of Entangled Hydroxyethyl Cellulose (HEC) Solutions

Jelena Dinic and Vivek Sharma*



Cite This: *Macromolecules* 2020, 53, 3424–3437



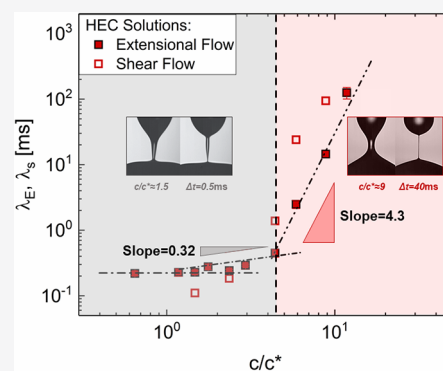
Read Online

ACCESS |

Metrics & More

Article Recommendations

ABSTRACT: Quantitative studies of capillarity-driven pinching and extensional rheology of aqueous solutions of polysaccharides like hydroxyethyl cellulose (HEC) are beyond the measurable range of most extensional rheometers, and are relatively rare, even though polysaccharides are widely used as rheology modifiers. In this study, we utilize dripping-onto-substrate (DoS) rheometry protocols that we recently developed to characterize the pinching dynamics and extensional rheology response of aqueous HEC solutions. We find that the radius evolution data from the pinching necks show an elastocapillary regime that can be fit to determine the extensional relaxation time even for unentangled HEC solutions that show neither rate-dependent regime in shear viscosity nor measurable elasticity in the shear rheology response measured using torsional rheometers. Furthermore, the radius evolution data for the entangled HEC solutions display a power law regime, previously reported only for multicomponent complex fluids containing particles, bubbles, drops, and lamellar gel networks described with the generalized Newtonian fluid models. However, the entangled HEC solutions that exhibit pronounced shear thinning and measurable elastic moduli also reveal that the power law in the radius evolution data is modulated in the late stage by viscoelastic effects, allowing the measurement of both extensional relaxation time and steady, terminal extensional viscosity. Finally, we show that the pinching dynamics underlying drop formation/liquid transfer of HEC solutions can be determined fairly accurately by measuring shear rheology response, unlike the solutions of flexible polymers that display a stark contrast in response to shear and extensional flows.



INTRODUCTION

Polysaccharides including hydroxyethyl cellulose (HEC) are often used as rheology modifiers^{1–7} in inks, paints and coatings,^{8–11} foods,^{7,12–15} pharmaceuticals,¹⁶ and cosmetics.^{8,9,17,18} At a relatively low concentration (typically <1 wt %), polysaccharides provide formulations with an enhanced zero shear viscosity and a well-defined shear thinning behavior.^{1–6} Enhanced viscosity at low shear rates increases the stability against flocculation or aggregation (and shelf life) and controls the spreading rate and area over a target substrate (e.g., skin for cosmetics, wall for paints, plates for food, or paper for inks). Likewise, adequate viscosity reduction facilitates mixing and pouring at intermediate shear rates ($10^0 < \dot{\gamma} < 10^2 \text{ s}^{-1}$) and facilitates liquid transfer to substrates at higher rates ($10^3 < \dot{\gamma} < 10^6 \text{ s}^{-1}$). Stickiness, tackiness, stringiness, cohesiveness, jettability, printability, and spinnability are often determined qualitatively by examining the pinching behavior of a liquid neck or filament stretched between finger and thumb, or between a rod and reservoir, or by visualizing dripping/jetting behavior.^{19–25} However, a quantitative assessment of such heuristic properties requires the understanding of interfacial flows and instabilities, as well

as material properties underlying pinching dynamics.^{22–29} In particular, characterizing and understanding the extensional rheology response assumes a critical significance as stream-wise velocity gradients associated with extensional strain, ϵ , and extensional strain rate, $\dot{\epsilon}$, spontaneously arise during capillarity-driven pinching of liquid filaments^{22–24} and near free surfaces in coating flows.³⁰ In this study, we introduce capillarity-driven pinching in lieu of the conventionally used term “capillary thinning and breakup” (or “capillary thinning and pinch-off”) to avoid confusion with (shear) thinning measured using capillary rheometers.³¹ It is well established that the extensional rheology response exhibits a high sensitivity to deformation history, revealing a distinct behavior based on the experimental protocol used.^{32–36} Therefore, the analysis of pinching dynamics provides access to extensional rheology

Received: January 14, 2020

Revised: April 12, 2020

Published: April 29, 2020

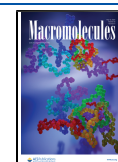


Table 1. Shear and Extensional Rheology of Aqueous HEC Solutions

authors (year)	shear or extension	M_w [kg/mol]	c [wt %]	remarks	refs
Naik et al. (1976)	shear	550	0.5–1.5	effect of concentration, c , and temperature, T	71
Tanaka et al. (1990)	shear	250	0.02–0.5	contrasts HEC to hmHEC	72
Meadows et al. (1995)	both	64, 190, 450	varying	extensional thinning measured using opposed jets	73
Maestro et al. (2002)	shear	90, 1300	all conc. regimes	compares HEC to hmHEC, uses Cross model fits	74
Patruyo et al. (2002)	both	300, 560	varying	compares HEC to hmHEC (and the influence of SDS)	75
Laschet et al. (2004)	shear	400, 1100, 1200, 1300	all conc. regimes	contrasts the influence of surfactants on HEC and hmHEC solutions	76
Arfin et al. (2012)	shear	90, 720, 1300	all conc. regimes	reports the formation of HEC fibers	79
Vadodaria et al. (2016)	shear	720	varying	discusses empirical methods for the determination of intrinsic viscosity	80
Vadodaria et al. (2016)	extension	720	1, 1.5, 2	shows sensitivity to step strain in CaBER measurements	36
Del Giudice et al. (2017)	shear	250	all conc. regimes	employs multiple techniques to measure similar concentration dependence for specific viscosity and relaxation time	81

response at strain rates most relevant for liquid transfer applications.^{11–16,22–24,37–49} Even though the shear rheology of polysaccharide solutions is well studied,^{1–9} pinching dynamics and extensional rheology are relatively less well characterized due to long-standing challenges summarized and addressed in this study.

For simple, Newtonian fluids, the extensional viscosity is merely 3 times the shear viscosity or $\eta_E = 3\eta$. In contrast, the extensional viscosity of polymer solutions (especially dilute solutions of flexible polymers) can be orders of magnitude higher than the shear viscosity,^{23,24,30–33,45–49} and $\eta_E(\epsilon, \dot{\epsilon})$ can show strain hardening even if the steady shear viscosity, $\eta(\dot{\gamma})$, exhibits shear thinning. The interplay of inertial, viscous, and capillary stresses dictates the pinching dynamics for Newtonian fluids.^{24–29} For polymeric complex fluids, the macromolecular response to extensional flows within a pinching neck (or filament) contributes additional viscoelastic stresses that influence pinching dynamics and filament life span (or pinch-off time). For flexible polymer solutions, the radius evolution data for pinching necks exhibit an initial inertio-capillary (IC) or visco-capillary (VC) regime followed by the elastocapillary (EC) regime with an exponentially slow decrease in radius or $R(t) \propto \exp(-t/\lambda_E)$ anticipated by the analysis based on Oldroyd-B, Giesekus, or FENE-P models.^{11–15,22–24,37–59} The most commonly used protocols^{24,25,39–44,60–62} involve the analysis of radius evolution of a neck created by applying a step strain to a liquid bridge formed between two parallel plates. However the protocol, also implemented in a commercially available technique called capillary breakup extensional rheometer (CaBER)^{11,34,61–63} presents three key challenges: (i) pinch-off is completed before the plate separation occurs for low-viscosity ($\eta < 50$ mPa·s) or low-elasticity (relaxation time, $\lambda < 1$ ms) fluids,^{62,64} (ii) initial step strain influences the pinching dynamics for micro-structured materials,^{34–36} and (iii) the transition from an initial IC/VC to EC regime is often not observed. Consequently, the few studies that rely on stretched liquid bridge (or CaBER) utilized high-molecular-weight (typical $M_w > 10^6$ Da) solutions at high concentrations ($c > 0.5$ wt % or $c > c^*$ or the overlap concentration),^{12–14,35,40,43,65–70} even though lower concentrations and molecular weights are often used in practice. For example, among the selected rheological

characterization studies listed in Table 1 for solutions of HEC and its hydrophobically modified analogue or hmHEC,^{36,71–78} the only CaBER measurements were limited to $c = 1, 1.5,$ and 2 wt % ($M_w = 7.2 \times 10^5$ g/mol) and showed a high sensitivity to the initial step strain.³⁶

In this study, we characterize the shear and extensional rheology response of both dilute and nondilute aqueous HEC solutions prepared with $M_w = 7.2 \times 10^5$ g/mol and $M_w = 1.3 \times 10^6$ g/mol. We characterize the pinching dynamics and extensional rheology response of HEC solutions using dripping-onto-substrate (DoS) rheometry protocols^{45–49} that rely on the visualization and analysis of capillarity-driven pinching of a fluid neck formed between a nozzle and a sessile drop on a substrate. We have established that DoS rheometry protocols overcome the key limitations of CaBER, including characterization of low-viscosity ($\eta < 50$ mPa·s) or low-elasticity (relaxation time, $\lambda < 1$ ms) fluids.^{15,45–49} To the best of our knowledge, we present the first set of measurements of viscoelasticity and extensional rheology response for dilute polysaccharide solutions using analysis of pinching dynamics, even for solutions that exhibit neither shear thinning in steady shear nor measurable elastic modulus in oscillatory shear measurements carried out on torsional rheometers. A companion paper identifies the macromolecular parameters underlying the dramatic differences in the pinching dynamics of dilute HEC and poly(ethylene oxide) (PEO) solutions. Here, we primarily focus on the pinching dynamics of entangled aqueous HEC solutions that show an additional power law (PL) regime before the viscoelastic effects are manifested, in striking contrast to the typical IC/VC–EC transition displayed by solutions of flexible polymers. Though models based on the generalized Newtonian fluids anticipate a power law regime in radius evolution data,^{82–84} PL followed by viscoelastic response is neither expected from the existing theoretical models and simulations nor reported in previous experimental studies on complex fluids containing particles, bubbles, drops, and lamellar gel network.^{24,47,85,86} We contrast the power law exponents obtained using shear and extensional rheology measurements and elucidate the stretched polymer physics and rheological properties that make polysaccharides highly suitable rheology modifiers.

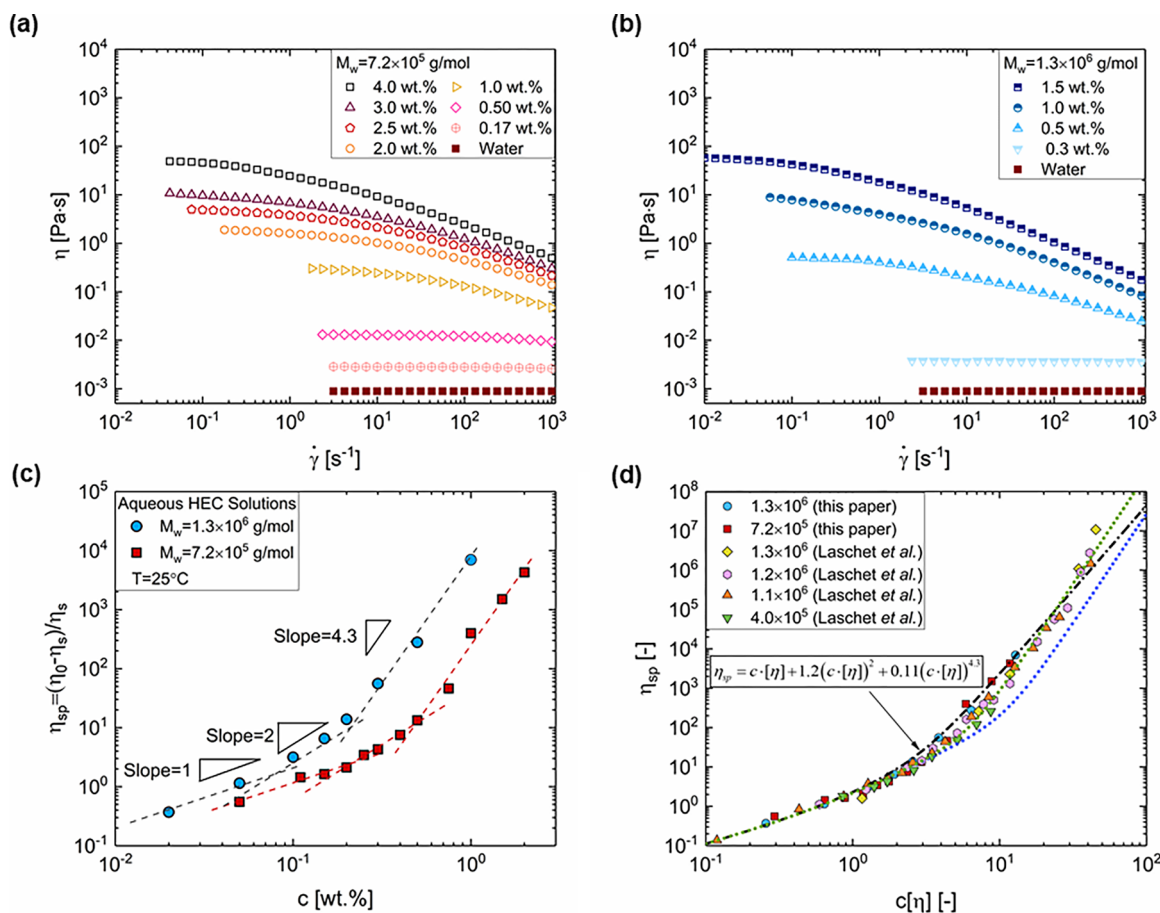


Figure 1. Shear rheology response of HEC solutions. Steady shear viscosity against shear rate of aqueous solutions of HEC with (a) $M_w = 7.2 \times 10^5$ g/mol and (b) $M_w = 1.3 \times 10^6$ g/mol. (c) Specific viscosity of aqueous HEC solutions for both molecular weights plotted as a function of polymer concentration exhibits three regimes: dilute, $\eta_{sp} \propto c$; semidilute regime, $\eta_{sp} \propto c^2$; and entangled regime, $\eta_{sp} \propto c^{4.3}$. (d) Robust agreement exists between specific viscosity plotted against dimensionless polymer concentration (as overlap concentration, $c^*[\eta] \approx 1$) for two molecular weights examined in this study, and additional datasets extracted from Laschet *et al.*^{3,76} However, our expression, shown as a black dashed-dotted line fit to our data differs from the expression [shown as green/blue dotted lines (see text)] obtained by Laschet *et al.*^{3,76}

MATERIALS AND METHODS

Aqueous solutions of 2-hydroxyethyl cellulose (HEC; Sigma-Aldrich, average molecular weight $M_w = 7.2 \times 10^5$ g/mol, and $M_w = 1.3 \times 10^6$ g/mol, both with molar substitution, M.S. = 2.5) were prepared by slowly adding a polymer in its as-received powder form to deionized water. The solutions are then placed on a roller for several days to achieve homogeneous mixing and to avoid high deformation rates that can lead to chain scission (though the influence is more pronounced for polymers with higher extensibility and flexibility). The shear rheology response of the polymer solutions was characterized using a concentric cylinder Couette cell for low-viscosity aqueous HEC solutions ($\eta_0 < 0.2$ Pa·s) and cone-and-plate geometry (50 mm diameter, 1° cone angle) for higher-viscosity aqueous solutions on an Anton Paar MCR 302 Rheometer (torque range, 10^{-5} –200 mN·m) at 25 °C. The steady shear viscosity, $\eta(\dot{\gamma}) = \tau/\dot{\gamma}$, was computed from the measured shear stress, τ , resulting from shear rates in the range of $\dot{\gamma} = 0.01$ – 10^3 s $^{-1}$.

The DoS rheometry setup comprises a dispensing system that includes a syringe pump connected to a nozzle with outer diameter $D_0 = 2R_0 = 1.27$ mm and inner diameter $D_i = 0.84$ mm. The imaging system consists of a light source with a diffuser and a high-speed camera (Fastcam SA3) with a train of lenses (Nikkor 3.1× zoom (18–25 mm) lens, plus a macro lens) attached for obtaining images with high magnification, and at high frame rate (typically 8000–20 000 fps). A finite volume of polymer solution is released from the nozzle onto a substrate placed at a constant height H from the nozzle (the aspect ratio selected was kept constant at $H/D_0 \approx 3$). A liquid

bridge is formed between the nozzle and the sessile drop formed on the substrate. The flow rate was also kept low and constant for all experiments ($Q = 0.02$ mL/min). The relatively slow release of drops onto a partially wetting substrate helps to decouple the neck thinning dynamics from the drop spreading dynamics and to relax any stresses accumulated in the nozzle. If needed, the contact line of the sessile drop can be pinned using a cylindrical plate as a substrate.⁸⁷ The DoS videos were analyzed using ImageJ⁸⁸ and MATLAB using specially written codes for edge detection and for the determination of neck radius as a function of time. Several recent papers from our group and others provide a detailed discussion of DoS rheometry protocols for characterizing pinching dynamics and extensional rheology response of neutral and charged polymer solutions,^{45–49,89–94} inks,^{47,95} linear and branched micellar solutions,^{47,87,96,97} as well as foods, cosmetics, and other yield stress fluids.⁴⁷

RESULTS AND DISCUSSION

Concentration-Dependent Steady Shear Viscosity Response of HEC Solutions. Steady shear viscosity as a function of shear rate data for aqueous HEC solutions plotted in Figure 1a,b was obtained using a torsional rheometer. For both molecular weights, the three highest concentrations of aqueous HEC solutions exhibit pronounced shear thinning at high shear rates, as shown in Figure 1a,b. As polymer concentration increases, the onset of shear thinning shifts toward lower values of shear rates, consistent with the expected

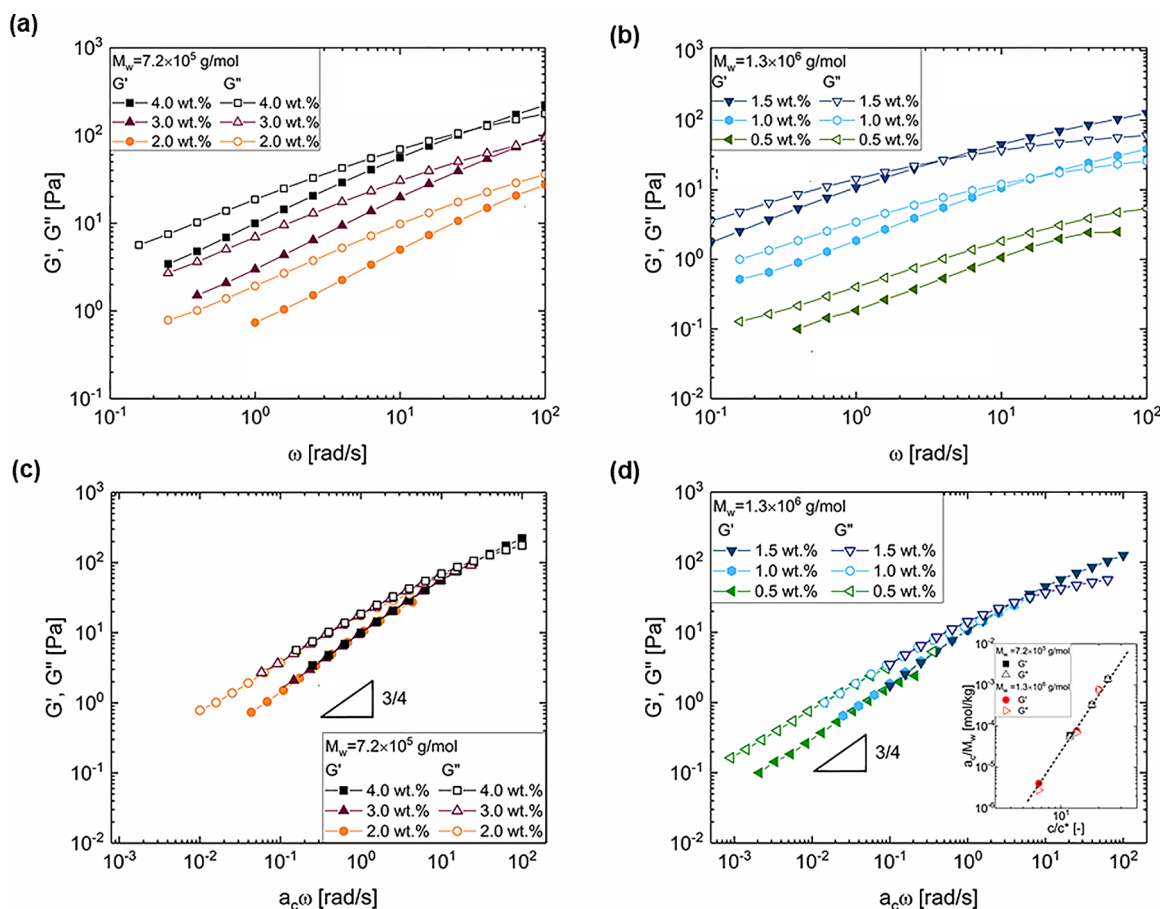


Figure 2. Oscillatory shear rheology response of the entangled HEC solutions. Storage (closed symbols) and loss (open symbols) moduli as a function of oscillation frequency of entangled solutions of HEC with (a) $M_w = 7.2 \times 10^5$ g/mol and (b) $M_w = 1.3 \times 10^6$ g/mol. (c, d) Superimposed datasets from (a, b). The horizontal shift factors, a_c , used for superimposing experimental datasets are shown in the inset of (d).

concentration-dependent increase in the shear relaxation time, λ_s . The rate-dependent variation in shear viscosity can be described using the following expression for the Cross model⁹⁸

$$\eta = \eta_\infty + \frac{\eta_0 - \eta_\infty}{1 + (\dot{\gamma}/\dot{\gamma}_c)^m} \quad (1)$$

where η_∞ represents the shear viscosity at a high shear rate, η_0 is the rate-independent zero shear viscosity, m is the Cross model exponent, and $\dot{\gamma}_c$ is the shear rate associated with the onset of power law regime. We assumed that the high shear rate viscosity equals solvent viscosity, i.e., $\eta_\infty = \eta_s$ reducing the number of fitting parameters to 3. Though Morris and co-workers^{99,100} report the exponent $m = 0.76$ for several polysaccharides, the values obtained from the fits to data shown in Figure 1 are neither equal to 0.76 nor constant.

The values of zero shear viscosity, η_0 , and known solvent viscosity, $\eta_s = 0.89$ mPa·s, are used to calculate the specific viscosity $\eta_{sp} = (\eta_0 - \eta_s)/\eta_s$ (also known as the relative viscosity increment), and the concentration with $\eta_{sp} = 1$ is utilized for determining the critical overlap concentration, $c^* = 0.17$ wt % for $M_w = 7.2 \times 10^5$ g/mol. Our c^* estimate is quite similar to $c^* = 0.14$ wt % reported by Arfin *et al.*⁷⁹ for HEC with matched molecular weight procured from the same supplier. Specific viscosity as a function of HEC concentration in aqueous solution exhibits three distinct regimes: $\eta_{sp} \propto c$ for the dilute regime ($c < c^*$), $\eta_{sp} \propto c^2$ in the semidilute, unentangled regime ($c < c^* < c_e$), and $\eta_{sp} \propto c^{4.3}$ in the entangled regime ($c >$

c_e), as shown in Figure 1c, where c_e refers to entanglement concentration. The nearly linear concentration dependence for dilute solutions is consistent with theory,^{101–103} and three similar regimes are reported for other polysaccharides.^{1–3,6,7,99,104,105} As intrinsic viscosity $[\eta]$ is a measure of coil size, and related to overlap concentration by $c^*[\eta] \approx 1$, the Berry number, $c[\eta]$, represents a dimensionless measure of degree of overlap. Intrinsic viscosity $\eta = 10$ dL/g measured for the higher $M_w = 1.3 \times 10^6$ g/mol is higher than $\eta = 5.98$ dL/g measured for $M_w = 7.2 \times 10^5$ g/mol.

The concentration-dependent specific viscosity for semidilute, entangled HEC solutions ($c > c_e$) displays a relatively high exponent of 4.3 as in $\eta_{sp} \propto c^{4.3}$ (see Figure 1c) that agrees well with $\eta_{sp} \sim c^{4.2}$ reported by Del Giudice *et al.*⁸¹ Similar strong exponents are obtained for the exhaustive range of uncharged polysaccharides, including dextrans, locust bean gum, and alginate, as tabulated by Morris *et al.*,⁹⁹ and for many cellulose esters and ethers tabulated by Clasen and Kulicke,³ among others.^{1,2} The presence of hydrophobic groups and/or hydrogen bonding³ provide additional interactions between the polysaccharides, leading to a stronger exponent than expected from theory for semidilute entangled polymer solutions.^{101,102} Figure 1d shows that our specific viscosity data can be overlaid onto the datasets of Laschet *et al.*⁷⁶ Our data can be fit with the expression $\eta_{sp} = c[\eta] + 1.2(c[\eta])^2 + 0.11(c[\eta])^{4.3}$ shown as the dashed-dotted line. Laschet *et al.* obtained a higher exponent of 5.56 as their fit (shown as a dotted line) corresponding to the expression $\eta_{sp} = c[\eta] +$

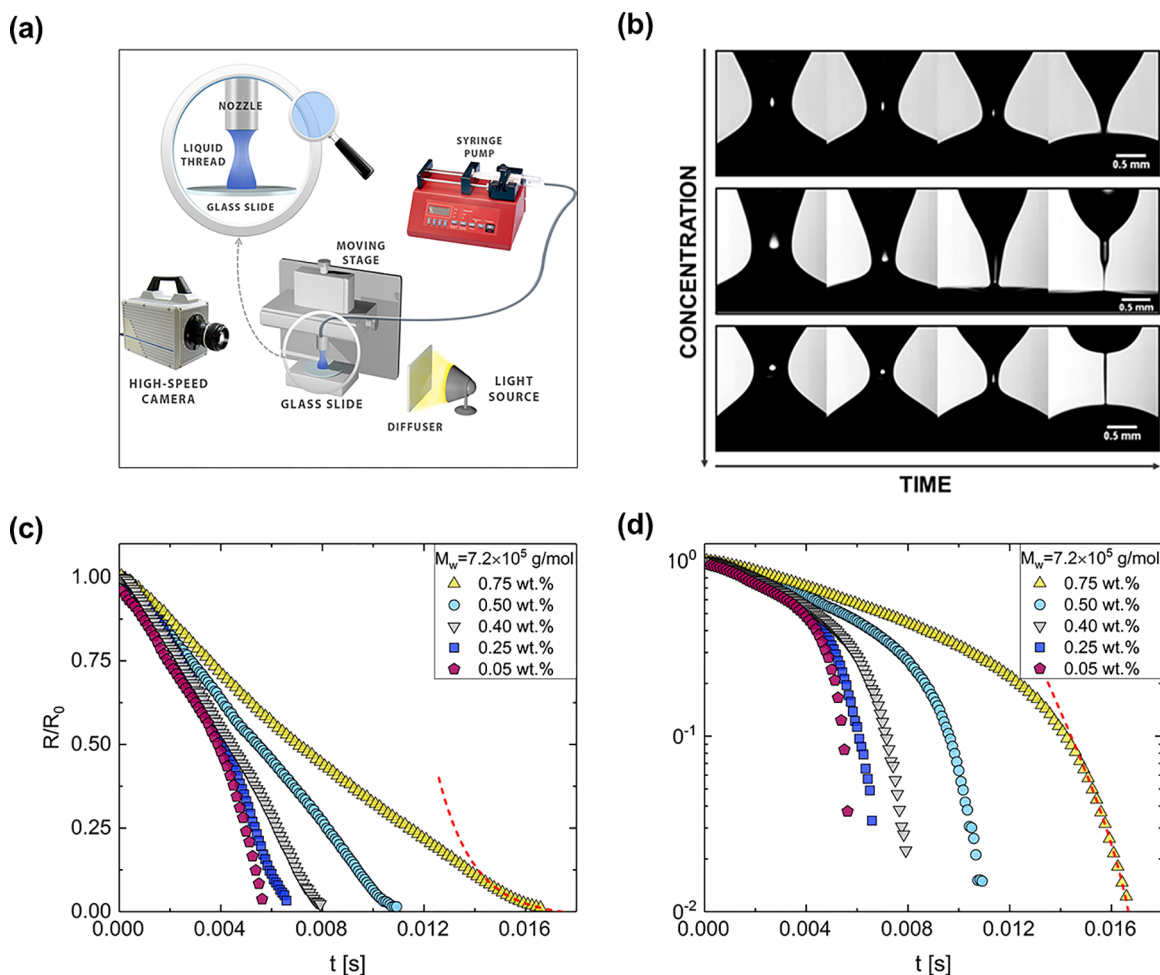


Figure 3. Dripping-onto-substrate (DoS) rheometry experimental setup and sequence of images showing neck shape evolution for aqueous HEC solutions. (a) DoS experimental setup consists of a high-speed camera with attached lenses and a dispensing system used for releasing a small volume of fluid onto a glass substrate. (b) Image sequences for aqueous solutions of HEC ($M_w = 7.2 \times 10^5$ g/mol) with $c = 0, 0.25,$ and 0.4 wt % show a transition from the conical shape obtained for water to a slender filament obtained for 0.4 wt %. Time steps between successive two images for montages of the HEC solutions with $c = 0, 0.25,$ and 0.4 wt % are equal to $\Delta t = 0.3, 1,$ and 1 ms, respectively. (c) Radius evolution in time for one dilute solution ($c = 0.05$ wt %), three semidilute HEC solutions ($c = 0.25, 0.4, 0.5$ wt %), and one solution in the entangled regime ($c = 0.75$ wt %) plotted on a linear-linear plot displays a short elastocapillary regime close to the pinch-off. (d) Radius evolution data from (c) are replotted using semilog axes. The dashed line shows the fit obtained using eq 7.

$1.2(c[\eta])^2 + 0.205 \cdot 10^{-3}(c[\eta])^{5.56}$ is based on data that include much higher concentrations than probed in our measurements. We find that using $2.05 \cdot 10^{-3}$ as prefactor (green dotted line) in place of $0.205 \cdot 10^{-3}$ (blue dotted line) provides a better fit to their entire dataset.

Oscillatory Shear Response of Aqueous HEC Solutions. The frequency-dependent storage modulus, $G'(\omega)$, and loss modulus, $G''(\omega)$, for the entangled HEC solutions shown in Figure 2 were measured at a strain amplitude of 5% (selection of a small amplitude was based on the strain amplitude sweep, not shown here). The frequency-dependent moduli values shown in Figure 2a,b reveal that the solutions behave neither like viscoelastic liquids that are expected to show $G'(\omega) \propto \omega^2$ and $G''(\omega) \propto \omega$ nor like gels that exhibit frequency-independent $G'(\omega) \propto \omega^0$. At the lowest frequencies characterized, $G'(\omega)$ and $G''(\omega)$ values seem to show the same slope, but with $G' < G''$ (liquidlike response). On visual inspection, the highest-concentration solution appears to be highly viscous and physical gel-like. The datasets for these highly entangled systems appear to be self-similar, and in Figure 2c,d, we show that a master curve can be obtained using

time-concentration superposition plots. The concentration-dependent scaled shift factors, a_c , plotted in the inset in Figure 2d show a power law exponent of $\alpha = 4.5$. The superimposed plots reveal a frequency dependence of $\omega^{3/4}$ for both moduli, consistent with the high-frequency response anticipated for entangled semiflexible polymers based on theoretical models^{106–109} as well as previous experimental results for actin networks,^{109,110} cellulose in ionic liquids,¹⁰⁵ and rodlike fd-virus suspensions,¹¹¹ among others. The corresponding moduli values were below the instrument resolution for the unentangled aqueous HEC solutions that have relatively low viscosity (and no measurable elasticity).

Shape and Shape Evolution of Necks Undergoing Capillarity-Driven Pinching. The DoS rheometry setup schematically shown in Figure 3a was used to visualize and analyze the evolution of neck shape for aqueous HEC solutions. Representative image sequences included in Figure 3b begin with the same, matched scaled radius, and the time intervals between the chosen four snapshots are $\Delta t = 0.3$ ms for water and $\Delta t = 1$ ms for the two polymer solutions. A close examination of the image sequences (Figure 3b) for the

aqueous HEC solutions as a function of polymer concentration shows that a pronounced conical neck persists even in the semidilute regime. The conical-shaped neck is characteristic inertio-capillary (IC) response associated with the neck pinching dynamics of low-viscosity (inviscid) fluids like water. Using Rayleigh time, $t_R = (\rho R_0^3/\sigma)^{1/2}$, as the characteristic timescale for inertio-capillary pinching^{26,112,113} (computed using density, ρ , and surface tension, σ), the radius evolution data for IC response follow a viscosity-independent, power law expression^{26,27,114,115}

$$\frac{R(t)}{R_0} = X \left(\frac{t_f - t}{t_R} \right)^{2/3} \quad (2)$$

Though the prefactor X is often quoted to have a value of either 0.8 or 0.65, we recently found that both experiments and volume-of-fluid (VOF)-based numerical simulations yield a lower value of $X = 0.4$ for glycerol–water solutions (similar viscosity range as data included in Figure 3).¹¹⁶ Deblais *et al.*¹¹⁷ also found a range of values $X = 0.4$ – 0.6 (influenced by fluid viscosity).

The conical shape is absent and replaced by a slender cylindrical neck for the HEC solution with $c = 0.4$ wt %, as shown in Figure 3b. The slender filament that emerges in the last stage before breakup of HEC solutions at concentrations close to overlap concentration for the chosen molecular weight would be missed entirely in the commercial CaBER devices that use a laser micrometer to characterize the diameter of the pinching neck in a plane fixed halfway between the two plates. Moreover, as the typical CaBER protocols require ~ 50 ms to stretch the liquid bridge, and the filament time span of the HEC solution at $c/c^* = 3$ is only $t_f = 40$ ms, such characterization for unentangled solutions is not possible on a conventional CaBER. Both the neck shape and radius evolution data shown in Figure 3c,d for the aqueous HEC solution for unentangled solutions display a change in pinching behavior, relatively close to the pinch-off event. The neck shape appears to become more slender as the concentration increases. The slender cylindrical neck can form in four scenarios, summarized next.

Pinching Dynamics of Slender, Cylindrical Necks: Four Scenarios. Scenario (i) arises for high-viscosity Newtonian fluids undergoing viscocapillary pinching^{24,118} with characteristic viscocapillary time, $t_{vc} = \eta R_0/\sigma$, and the expression shown below

$$\frac{R}{R_0} = 0.0709 \left(\frac{t_f - t}{t_{vc}} \right) \quad (3)$$

The relative importance of viscous and inertio-capillary effects can be evaluated by computing the Ohnesorge number, $Oh = t_{vc}/t_R = \eta/\sqrt{\rho\sigma R_0}$ or the ratio of the characteristic timescale for VC and IC responses. As VC response is expected for $Oh > 1$, the unentangled solutions are all anticipated to show the IC regime. The magnitude of Rayleigh time for aqueous polymer solutions is $t_R \sim 2$ ms.

Scenario (ii) is manifested by viscoelastic fluids undergoing elastocapillary (EC) pinching characterized by an exponentially slow decrease in radius, captured by the following expression

$$\frac{R(t)}{R_0} \approx \left(\frac{G_E R_0}{2\sigma} \right)^{1/3} \exp\left(-\frac{t - t_c}{3\lambda_E}\right) \quad (4)$$

Equation 4 differs from the most often cited Entov and Hinch expression⁵⁰ in utilizing the extensional relaxation time, λ_E , as a timescale in contrast to longest shear relaxation time, λ_s . Also, the timescale is shifted such that t_c defines the onset of EC regime and G_E represents an apparent extensional modulus (in lieu of $G = (\eta_0 - \eta_s)/\lambda$ used by Entov and Hinch⁵⁰ and others). Elastic effects manifest for low Oh if Deborah number $De = \lambda/t_R > 1$ and for high Oh if $\lambda/t_{vc} > 1$.

Scenario (iii) arises for shear thinning fluids that display a power law exponent of $n > 0.66$. The radius in this case decreases as a power law^{47,82,84} captured by the expression below

$$\frac{R(t)}{R_0} = Y (t_f - t)^n = \left(\frac{t_f - t}{t_{PL}} \right)^n \quad (5)$$

where the exponent n is associated with the power law model commonly used to describe the variation of shear stress $\tau = K\dot{\gamma}^n$ with shear rate using the flow consistency, K . In the high-shear-rate regime, steady shear viscosity data (Figure 1) can provide the values of n . Doshi *et al.*⁸² showed that for $n > 0.66$, the prefactor $Y = \Phi(n)\sigma/K$, where $\Phi(n)$ is a constant that depends on n .^{24,47,82–84} Though radius evolution displays a power law for shear thinning fluids with exponent $n < 0.6$ as well, in such cases, the neck is not slender and two conical necks are observed before the pinch-off event. The existence of two cones was predicted from numerical computations by Suryo and Basaran⁸⁴ and was termed as nonslender viscous power law (NSVP) scaling, but the value of Y was not provided. We rewrite the prefactor $Y = \Phi(n)\sigma/K = t_{PL}^{-n}$ to identify the timescale t_{PL} as the characteristic timescale for power law fluids.

Scenario (iv) arises for viscoelastic fluids with finite extensibility, as the interplay of nonlinear viscoelasticity and capillarity can lead to a terminal viscoelastocapillary response (TVEC) such that the radius evolution follows a linear decrease captured by the expression^{24,119} given below

$$\frac{R(t)}{R_0} = \frac{\sigma}{2R_0\eta_E} (t_f - t) = \frac{1/2}{OhTr^\infty} \left(\frac{t_f - t}{t_R} \right) \quad (6)$$

Here, $Tr^\infty = \eta_E^\infty/\eta_0$ is the terminal Trouton ratio and t_f refers to the filament life span. In such cases, a strain as well as strain-rate-independent steady, terminal extensional viscosity η_E^∞ can be determined from radius evolution data. The finite extensibility response captured by eq 6 arises after the stress contributed by highly stretched and oriented macromolecules saturates.^{11,40,43,48,89} As $Tr^\infty \gg 3$ for flexible polymers,^{24,40,43,46,48} the pinch-off event is significantly delayed compared to Newtonian fluids. Nearly all experimental studies^{3,12–14,22,24,25,34–70,87,89–93,95–97,120–128} extract an extensional relaxation time, λ_E , from the EC regime, and less frequently, a terminal viscoelastocapillary (TVEC) regime with a linear decrease in radius yields measurement of a strain as well as rate-independent steady, terminal extensional viscosity, η_E^∞ .

An exponential decay in radius (a signature of an elastocapillary response) can be discerned in a linear–linear plot as shown in Figure 3c for unentangled HEC solutions with concentrations $c = 0.05, 0.25, 0.4,$ and 0.5 wt % for $M_w = 7.2 \times 10^5$ g/mol. Thus, these datasets exhibit an elastocapillary response, even though no elasticity is manifested in the corresponding oscillatory shear measurements (see Figure 2)

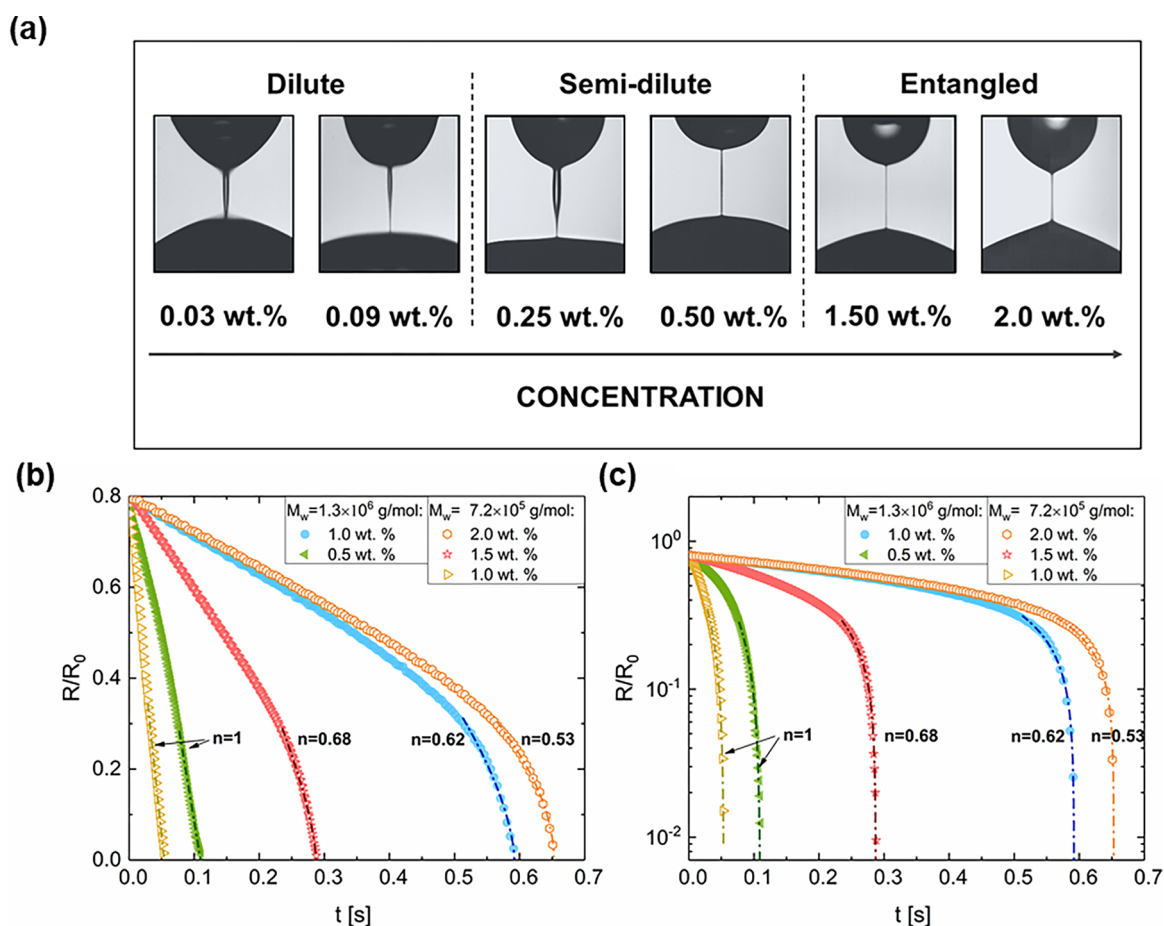


Figure 4. Filament shapes before pinch-off for a range of HEC solutions and the corresponding radius evolution data for entangled HEC solutions. (a) The images shown are the respective last snapshots with a continuous visible filament for HEC in all three concentration regimes. As the concentration of polymer increases, the shape of the filament becomes progressively slender. (b) Radius evolution as a function of time for HEC concentrations above the entanglement concentration, c_e , appears to be dominated by the power law behavior. (c) Radius evolution data from (b) are replotted using semilog axis, and several entangled solutions show power law exponent, $n < 0.66$.

and the steady shear viscosity values too appear rate-independent (see Figure 1). We previously reported the existence of similar short-lived elastocapillary regions (or tails) in the radius evolution data for solutions of a strong polyelectrolyte, sodium polystyrene sulfonate (NaPSS).⁴⁸ The radius evolution plots are replotted in Figure 3d on semilog axes following the standard procedure used in typical capillary breakup studies.^{42,62} In the radius evolution data for flexible polymer solutions including PEO solutions, a pronounced elastocapillary regime can be observed that contributes to a substantial delay in pinch-off.⁴⁹ In contrast, the addition of HEC only influences the last stage before breakup. However, the short-span elastocapillary regime seems to suppress satellite drop formation, though without increasing stringiness or stickiness, making polysaccharides ideal additives for drop formation and liquid transfer applications. A detailed investigation of the differences in macromolecular physics and dynamics between HEC and a model flexible polymer, PEO, is included in a companion paper, in which we identify the macromolecular parameters that can be tuned through chemistry to influence pinch-off dynamics, the extensional rheology response, and processability.

Power Law Response in Pinching Dynamics, Modulated by Viscoelasticity. The neck shape becomes quite slender as the concentration is increased above the overlap

concentration to entangled regime for HEC solutions, as shown in Figure 4a, and the filament life span (or the overall pinch-off time) is substantially longer. The comparison between 0.75 and 1.5 wt % data shown in Figures 3 and 4, respectively, reveals a 10-fold increase in filament life span, illustrating a pronounced shift in macromolecular dynamics from unentangled to entangled regime. Furthermore, as the entangled polymer solutions are strongly shear thinning, the radius evolution profile appears to follow the pinching dynamics known to be characteristic of power law fluids.^{47,82,84} Here, n exponent decreases with increasing concentration of polymer with any molecular weight ($0.5 \leq n \leq 1$ for the concentrations shown). The neck shapes present in the respective last snapshots with a continuous visible filament for HEC undergoing power law pinching appear to have a slender, cylindrical shape. However, for power law fluids with $n < 0.6$, numerical simulations by Suryo and Basaran⁸⁴ and experiments (with highly shear thinning fluid including food and cosmetics formulations) show neck shapes with two sharply outlined cones, touching at the midpoint of a pinching filament visualized just before the pinch-off event.^{47,85,86} Thus, the filament shape and shape evolution for the HEC solutions is not consistent with the typical power law thinning behavior. Likewise, even though the power law fits to the radius evolution data for two aqueous HEC solutions at $c = 1$ wt %

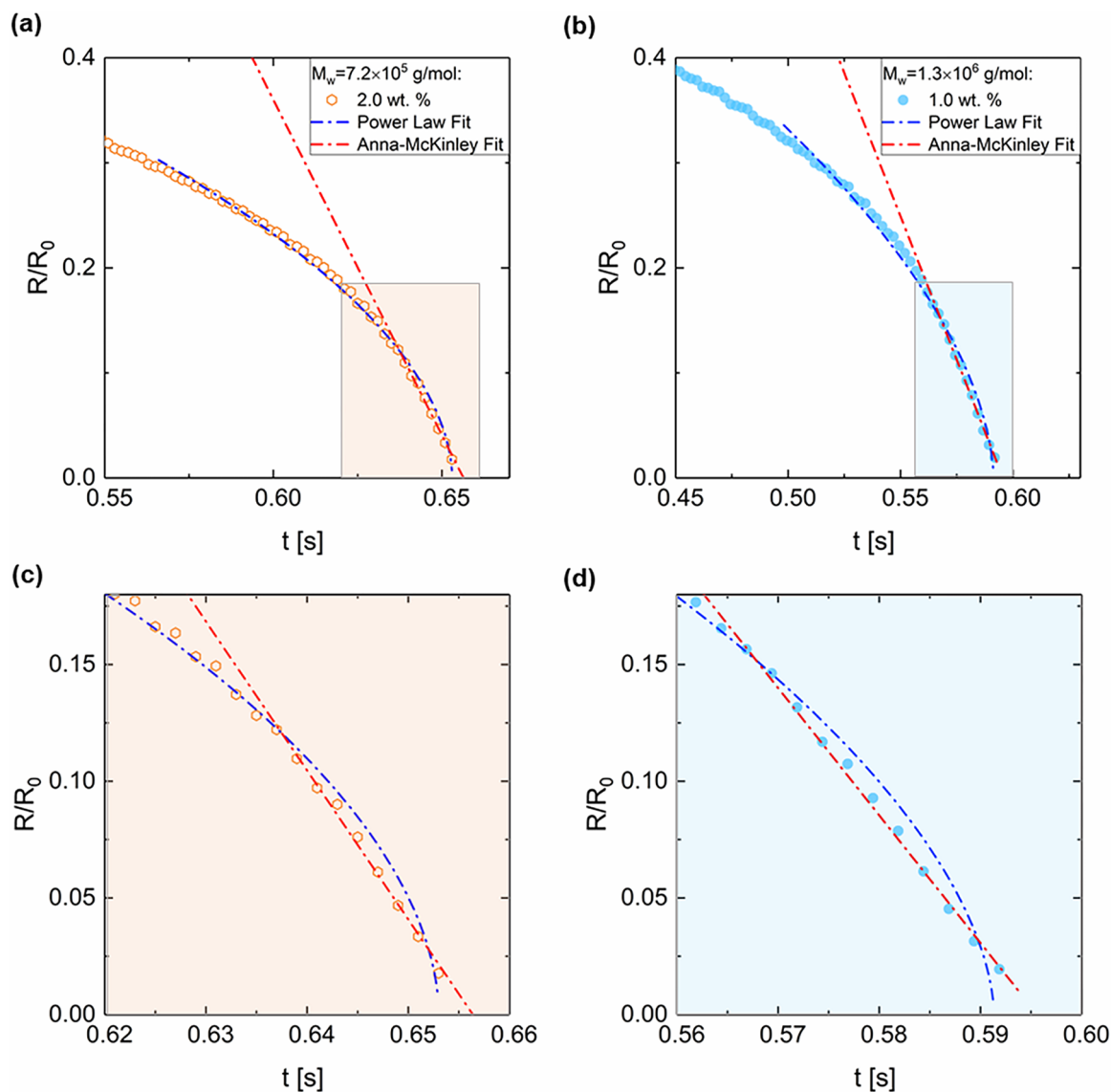


Figure 5. Concentration-dependent radius evolution data for entangled HEC solutions. (a, b) Fits to both power law and Anna–McKinley fitting equation are shown for one concentration each for $M_w = 7.2 \times 10^5$ g/mol and $M_w = 1.3 \times 10^6$ g/mol, respectively. (c, d) Plots of the zoomed-in regions indicated in (a, b) in light orange and blue are shown. While a power law fit appears to describe the radius evolution data for the HEC solutions quite well, deviation from the power law fit can be observed close to the pinch-off event (usually for $R/R_0 < 10^{-1}$). The radius evolution data in this region can be fit more accurately using the Anna–McKinley expression.⁴²

Table 2. Concentration-Dependent Variation in Parameters Characterizing the Shear and Extensional Rheology Response^a

M_w [kg/mol]	c [wt %]	λ_s [s]	η_0 [Pa·s]	Oh [–]	λ_E [s]	η_E^∞ [Pa·s]	t_f [s]
720	0.17	/ *	0.0022	0.011	2.2×10^{-4}	0.40	4×10^{-3}
720	0.25	1.1×10^{-4}	0.0040	0.020	2.3×10^{-4}	0.40	4.5×10^{-3}
720	0.40	1.9×10^{-4}	0.0077	0.039	2.4×10^{-4}	0.50	6.0×10^{-3}
720	0.50	2.9×10^{-4}	0.013	0.066	2.9×10^{-4}	0.90	1.0×10^{-2}
720	0.75	1.4×10^{-3}	0.043	0.22	4.5×10^{-4}	1.7	1.4×10^{-2}
720	1.0	2.4×10^{-2}	0.36	1.8	2.5×10^{-3}	4.0	5.4×10^{-2}
720	1.5	9.4×10^{-2}	1.4	7.1	1.5×10^{-2}	7.1	2.9×10^{-1}
720	2.0	1.5×10^{-1}	3.8	19	1.2×10^{-1}	8.5	6.5×10^{-1}
1300	0.1	2.3×10^{-4}	0.0037	0.019	3.7×10^{-4}	2.1	7.8×10^{-3}
1300	0.5	4.7×10^{-2}	0.25	1.3	2.4×10^{-3}	6.8	1.1×10^{-1}
1300	1	6.2×10^{-1}	6.2	31	6.7×10^{-2}	7.4	5.9×10^{-1}

^aThe filament life span was calculated with the initial dimensionless radius value of $R/R_0 = 0.8$ for all concentrations.

yield an exponent of $n = 1$ expected for constant viscosity Newtonian fluids, the polymer solutions show a pronounced

shear thinning (see steady shear viscosity data included in Figure 1).

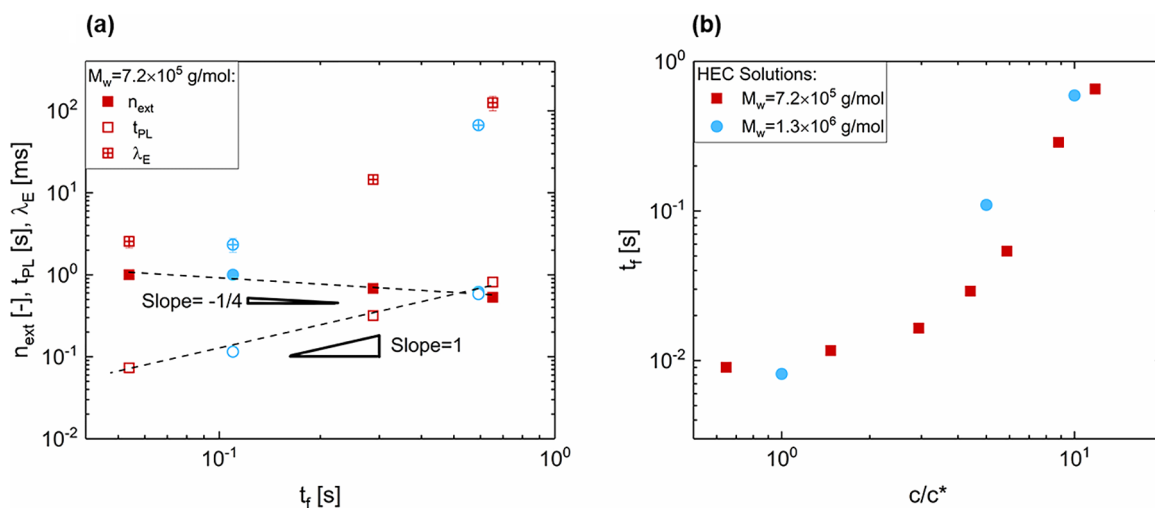


Figure 6. Correlation between filament life span and the parameters determined from the analysis of the filament radius evolution data for entangled HEC solutions. (a) Values of extensional relaxation time, λ_E [ms], and power law timescale, t_{PL} [s] (shown in open symbols), progressively increase in proportion to an increase in the filament life span, t_f [s]. In contrast, the power law exponent, n_{ext} (filled symbols), decreases as t_f (and polymer concentration) increases. (b) Filament life span, t_f , increases sharply with scaled concentration in the entangled regime that corresponds to $c/c^* > 3$.

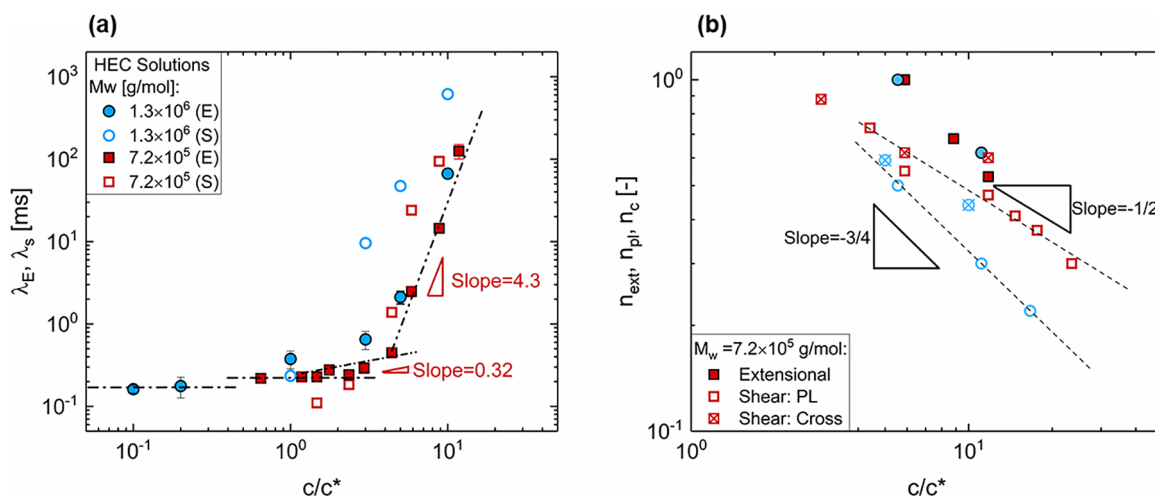


Figure 7. Relaxation times and power law exponents for aqueous HEC solutions: comparison between shear and extensional rheology response. (a) Extensional relaxation time, λ_E (filled symbols), as a function of HEC concentration showing three distinct scaling exponents of 0, 0.32, and 4.3. The shear relaxation time, λ_s , values (open symbols) were obtained using Cross model fits to the steady shear viscosity data. (b) Values of the exponent n_{ext} (filled symbols) extracted from fitting the radius evolution data with power law (eq 5) as a function of scaled HEC concentration are shown for both molecular weights. The n_{ext} values are contrasted with the exponents obtained using Cross model, n_c (crossed symbols), as well as power law model, n_{PL} (open symbols), to describe the shear thinning behavior of the HEC solutions.

The radius evolution data for power law fluids including emulsions, particle suspensions, carbopol gels, conditioner, foams, paints, etc. investigated before using DoS rheometry⁴⁷ and CaBER^{85,86} can be captured by eq 5, right up to the pinch-off event. However, on close inspection, we find that the power law model does not capture the radius evolution data near pinch-off, and viscoelastic effects manifest at the last stage, as shown in Figure 5. We find that the radius evolution data for the entangled polymer solutions investigated here manifest a short, elastocapillary response that can be fit (as shown in Figure 5c,d) using the semiempirical expression proposed by Anna and McKinley⁴²

$$\frac{R(t)}{R_0} = A \exp(-Bt) - Ct + D \quad (7)$$

Here, the parameter B can be interpreted as a measure of the longest relaxation time (approximately $B \approx 1/3\lambda_E$), while the parameter C ($\approx \sigma/2\eta_E^\infty R_0$) can be used for determining the steady, terminal extensional viscosity value. Equation 7 is utilized to fit the radius evolution data for polymer solutions,^{15,42,90,129,130} micellar solutions,^{34,97,131–133} and other complex fluids^{134,135} as it conveniently provides values of both λ_E and η_E^∞ (and facilitates the determination of strain rate and transient extensional viscosity). The values obtained from the torsional shear rheology and DoS rheometry characterization are listed in Table 2.

The majority of published studies rely on the study of pinching dynamics and extensional rheology response of the solution of high-molecular-weight flexible polymers like poly(ethylene oxide) (PEO), polyacrylamide (PAM), and polystyrene (PS) solutions. However, the fits included in

Figure 4 show that the elastocapillary span and finite extensibility (TVEC) regime for the HEC solutions constitute a significantly shorter fraction of the total filament life span, and hence the viscoelastic response can be easily missed in the analysis unless the frame rate is relatively high to capture the last regime where pinching rate increases dramatically. The existence of a similar power law regime, followed by the EC regime, is mentioned for polymer solutions only in one study by Clasen for semidilute polystyrene solutions.¹³⁶

The values listed in Table 2 show that the steady terminal extensional viscosity, η_E^∞ , increases with HEC concentration. However, for nondilute systems ($c > c^*$), the terminal Trouton ratio, $\text{Tr}^\infty = \eta_E^\infty/\eta_0$, decreases with the concentration for both polymers. The HEC with a lower $M_w = 7.2 \times 10^5$ g/mol displays $\text{Tr}^\infty \approx 180$ at the overlap concentration ($c^* = 0.17$ wt %) of solution and mere a $\text{Tr}^\infty = 5$ for 1.5 wt % ($c/c^* = 9$; entangled). In contrast, HEC with $M_w = 1.3 \times 10^6$ g/mol exhibits $\text{Tr}^\infty \approx 568$ at $c^* = 0.1$ wt %, and $\text{Tr}^\infty \approx 1$ for $c = 1.0$ wt % ($c/c^* = 10$). Since the shear viscosity of unentangled solutions appears to be rate-independent, $\text{Tr}^\infty = \eta_E/\eta_0 \approx \eta_E/\eta$. However, as entangled solutions are highly shear thinning, $\text{Tr} \gg \text{Tr}^\infty$ is expected at high deformation rates typically encountered during processing. Finally, the pinch-off time, t_f (which also represents the filament life span) can be computed from the ratio $t_f = D/C$.

Three parameters, power law index (n_{ext}), power law timescale (t_{PL}), and extensional relaxation time (λ_E), obtained by the fits included in Figure 5 for entangled solutions are plotted as a function of filament life span, t_f , in Figure 6a, and the filament life span, t_f is shown as a function of scaled concentration in Figure 6b. The absolute value of the extensional relaxation time (shown in ms) is considerably shorter than the filament life span (shown in seconds) at each concentration, whereas the values of power law time ($t_{\text{PL}} = 1/Y^{1/n}$) are linearly correlated with the filament life span values. Finally, t_f increases by nearly 2 orders of magnitude as the concentration is increased by 10-fold above the overlap concentration, emulating the strong increase in the values of shear and extensional viscosities.

We find that the values of shear relaxation time, λ_s , evaluated using $\dot{\gamma}\lambda_s = 1$ (Cross model fits to data in Figure 1) show the same concentration-dependent variation as extensional relaxation time, λ_E (see Figure 7a), and the values obtained for semiflexible HEC solutions are relatively well matched in striking contrast to the datasets for entangled flexible polymers.^{61,63} The power law exponents obtained respectively from shear and extensional rheology characterization appear to show a qualitatively similar decrease with an increase in concentration (see Figure 7b). The exponents obtained from the power law fit as well as the Cross model are shown for solutions made with both molecular weights. The power law exponents are found to be lower for HEC solutions with a higher-molecular-weight polymer ($M_w = 1.3 \times 10^6$ g/mol).

The extensional relaxation time values for unentangled HEC solutions are weakly concentration-dependent, but the entangled solutions ($c > c_e$) exhibit a strong increase with concentration $\lambda_E \propto c^{4.3}$ that mimics the exponent observed for specific viscosity and shear relaxation time $\lambda_E \propto \lambda_s \propto \eta_{\text{sp}} \propto c^{4.3}$. Although Del Giudice *et al.*⁸¹ do not report the extensional relaxation time, the authors found that shear relaxation time of aqueous HEC solutions displays the same concentration dependence as specific viscosity, $\eta_{\text{sp}} \propto \lambda_s \propto c^{4.18}$. The observation of $\eta_{\text{sp}} \propto \lambda_E \propto c^\alpha$ is also consistent with the trends

noted in a DoS rheometer-based investigation of polyelectrolyte dynamics⁴⁸ and agrees well with results from Fujii *et al.*¹³⁷ who performed birefringence measurements of semiflexible hydroxypropyl cellulose (HPC) solutions of similar Kuhn segment size to the HEC used in this study. Fujii *et al.*¹³⁷ argued that the scaling behavior of semiflexible polymers is a consequence of the predominant role played by the rotational diffusion of chains in driving relaxation, or $\eta_{\text{sp}} \propto \frac{1}{D_r} \propto \lambda_E \propto \lambda_s$, where D_r represents the rotational diffusion coefficient.¹³⁷

CONCLUSIONS

We characterize the concentration-dependent variation in shear and extensional rheology response of aqueous HEC solutions prepared with $M_w = 7.2 \times 10^5$ g/mol and $M_w = 1.3 \times 10^6$ g/mol. Steady shear viscosity measurements are used for computing specific viscosity and obtaining an overlap concentration $c^* = 0.17$ wt %, intrinsic viscosity $[\eta] = 5.98$ dL/g, and entanglement concentration $c_e = 0.5$ wt % for HEC with $M_w = 7.2 \times 10^5$ g/mol. The corresponding values obtained for HEC with $M_w = 1.3 \times 10^6$ g/mol are $c^* = 0.1$ wt %, $[\eta] = 10$ dL/g, and $c_e = 0.2$ wt %. The steady shear viscosity values measured for entangled HEC solutions display a pronounced degree of shear thinning captured using the Cross model. We show that the radius evolution data for the entangled polysaccharide solutions display an unmistakable power law regime in pinching dynamics with $R(t) \propto (t_f - t)^n$. Even though the power law response in capillarity-driven pinching is anticipated by theoretical models based on generalized Newtonian fluids, previously, power law scaling in radius evolution was primarily reported for multicomponent complex fluids containing particles, bubbles, drops, and a lamellar gel network. We find that the radius evolution data for polysaccharide solutions obtained with DoS rheometry achieve measurements of both λ_E and η_E^∞ from the EC-TVEC regime for the entire range of concentrations, even though such measurements are inaccessible in CaBER for dilute HEC solutions. The additional EC-TVEC regime observed before pinch-off for radius evolution data dominated by power law regime is neither predicted by previous models nor characterized using previous experiments. Likewise, the typically used models for viscoelastic fluids (Oldroyd-B, Giesekus, and FENE-P) do not anticipate power law regime in the radius evolution data obtained from the visualization of capillarity-driven pinching for polymer solutions.

The power law exponents obtained from the fits to shear thinning response measured using torsional rheometry appear to be closely matched with exponents obtained by fits to the filament radius evolution data acquired using DoS rheometry. Furthermore, the filament life span correlates primarily with the parameters obtained by fitting the power law regime in the radius evolution data extracted from the DoS rheometry data, and elastocapillary span is relatively short compared to filament life span, whereas it makes the primary contribution for solutions of flexible polymers like PEO. We find that the extensional relaxation time for entangled HEC solutions displays a relatively strong concentration dependence that scales linearly with specific viscosity, as well as with shear relaxation time values obtained from the onset of shear thinning data. Finally, we hope that the protocols and principles outlined here will prove useful for increasing the use and applicability of water-soluble polymers. Due to the increasing emphasis on nonvolatile organic compound (non-

VOC) paints and coatings and the worldwide push toward sustainability, there is an increasing emphasis on using water-soluble polymers and bio-sourced polymers, turning it into a multi-billion-dollar industry.⁹ We anticipate that the current study on the rheological behavior of aqueous polysaccharide solutions will be an important starting point for future studies of multicomponent complex fluids like inks, paints, coatings, food, and cosmetics, wherein the contribution from colloidal particles (used as binders, e.g., latex and as pigments) and surfactants (used as dispersing agents)^{10,138–141} adds more complexity to the rheology and processability.

AUTHOR INFORMATION

Corresponding Author

Vivek Sharma – Department of Chemical Engineering, University of Illinois at Chicago, Chicago 60608, Illinois, United States; orcid.org/0000-0003-1152-1285; Email: viveks@uic.edu

Author

Jelena Dinic – Department of Chemical Engineering, University of Illinois at Chicago, Chicago 60608, Illinois, United States

Complete contact information is available at:
<https://pubs.acs.org/10.1021/acs.macromol.0c00077>

Notes

The authors declare no competing financial interest.

ACKNOWLEDGMENTS

V.S. acknowledges funding support by the College of Engineering and the Department of Chemical Engineering at the University of Illinois at Chicago. V.S. and J.D. acknowledge Prof. Amanda Marciel, Rice University; Prof. Samanvaya Srivastava, UCLA; and Prof. Naveen Reddy, U. Hasselt, and Carina Martinez, UIC, for a close reading of the manuscript. J.D. was supported by the start-up funds as well as a Teaching Assistantship offered by the Department of Chemistry at UIC. J.D. is currently affiliated with Argonne National Laboratory and Pritzker School of Molecular Engineering at the University of Chicago as a postdoctoral researcher supervised by Prof. Matt Tirrell. J.D. and V.S. acknowledge Alexandro Estrada, who carried out some of the complementary experiments as an undergraduate summer researcher. Finally, the inspired idea to use capillarity-driven pinching in place of capillary thinning and breakup or “capillary thinning and pinch-off dynamics” was formalized in a discussion between Prof. Randy Ewoldt, UIUC, and V.S., following a related discussion with Prof. Gareth McKinley, MIT, and Prof. Chris Macosko, University of Minnesota, and the authors acknowledge these discussions.

REFERENCES

- (1) Dumitriu, S. *Polysaccharides: Structural Diversity and Functional Versatility*; 2nd ed.; Marcel Dekker: New York, 2005.
- (2) Lapasin, R.; Priel, S. *Rheology of Industrial Polysaccharides: Theory and Applications*; Chapman & Hall: London, 1995.
- (3) Clasen, C.; Kulicke, W. M. Determination of viscoelastic and rheo-optical material functions of water-soluble cellulose derivatives. *Prog. Polym. Sci.* **2001**, *26*, 1839–1919.
- (4) Kaneda, I., *Rheology of Biological Soft Matter*; Springer: Tokyo, 2017.
- (5) Braun, D. D.; Rosen, M. R. *Rheology Modifiers Handbook: Practical Use and Application*; Elsevier, 2013.
- (6) Kamide, K. *Cellulose and Cellulose Derivatives: Molecular Characterization and its Applications*; Elsevier: Amsterdam, 2005.

- (7) Wüstenberg, T. *Cellulose and Cellulose Derivatives in the Food Industry: Fundamentals and Applications*; John Wiley & Sons, 2014.
- (8) Glass, J. E., *Water Soluble Polymers: Beauty with Performance*; American Chemical Society: Washington DC, 1986.
- (9) Williams, P. A. *Handbook of Industrial and Water Soluble Polymers*; Blackwell Publishing Ltd: Oxford, 2007.
- (10) Lambourne, R.; Striven, T. A. *Paint and Surface Coatings: Theory and Practice*; 2nd ed.; Woodhead Publishing Ltd: Cambridge, U. K., 1999.
- (11) Sharma, V.; Haward, S. J.; Serdy, J.; Keshavarz, B.; Soderlund, A.; Threlfall-Holmes, P.; McKinley, G. H. The rheology of aqueous solutions of Ethyl Hydroxy-Ethyl Cellulose (EHEC) and its hydrophobically modified Analogue (hMEHEC): Extensional flow response in capillary break-up, jetting (ROJER) and in a cross-slot extensional rheometer. *Soft Matter* **2015**, *11*, 3251–3270.
- (12) Duxenneuner, M. R.; Fischer, P.; Windhab, E. J.; Cooper-White, J. J. Extensional properties of hydroxypropyl hther guar gum solutions. *Biomacromolecules* **2008**, *9*, 2989–2996.
- (13) Torres, M. D.; Hallmark, B.; Wilson, D. I. Effect of concentration on shear and extensional rheology of guar gum solutions. *Food Hydrocolloids* **2014**, *40*, 85–95.
- (14) Torres, M. D.; Hallmark, B.; Wilson, D. I.; Hilliou, L. Natural Giesekek Fluids: Shear and Extensional Behavior of Food Gum Solutions in the Semidilute Regime. *AIChE J.* **2014**, *60*, 3902–3915.
- (15) Jimenez, L. N.; Marti'nez Narva'ez, C. D. V.; Sharma, V. Capillary breakup and extensional rheology response of food thickener cellulose gum (NaCMC) in salt-free and excess salt solutions. *Phys. Fluids* **2020**, *32*, No. 012113.
- (16) Morozova, S.; Schmidt, P. W.; Metaxas, A.; Bates, F. S.; Lodge, T. P.; Dutcher, C. S. Extensional flow behavior of methylcellulose solutions containing fibrils. *ACS Macro Lett.* **2018**, *7*, 347–352.
- (17) Savary, G.; Grisel, M.; Picard, C. Cosmetics and Personal Care Products. *Natural Polymers: Industry Techniques and Applications*; Olatunji, O., Ed.; Springer, 2016; pp 219–261.
- (18) Gilbert, L.; Loisel, V.; Savary, G.; Grisel, M.; Picard, C. Stretching properties of xanthan, carob, modified guar and celluloses in cosmetic emulsions. *Carbohydr. Polym.* **2013**, *93*, 644–650.
- (19) Trouton, F. T. On the coefficient of viscous traction and its relation to that of viscosity. *Proc. R. Soc. London, Ser. A* **1906**, *77*, 426–440.
- (20) Fano, G. Contributo allo studio dei corpi filanti. *Arch. Fisiol.* **1908**, *5*, 365–370.
- (21) Green, H. The tackmeter, an instrument for analyzing and measuring tack: application to printing inks. *Ind. Eng. Chem., Anal. Ed.* **1941**, *13*, 632–639.
- (22) Yarin, A. L. *Free Liquid Jets and Films: Hydrodynamics and Rheology*; Longman Scientific & Technical, 1993.
- (23) Petrie, C. J. S. One hundred years of extensional flow. *J. Non-Newtonian Fluid Mech.* **2006**, *137*, 1–14.
- (24) McKinley, G. H. Visco-elasto-capillary thinning and break-up of complex fluids. *Rheol. Rev.* **2005**, *1*–48.
- (25) Bhat, P. P.; Appathurai, S.; Harris, M. T.; Pasquali, M.; McKinley, G. H.; Basaran, O. A. Formation of beads-on-a-string structures during break-up of viscoelastic filaments. *Nat. Phys.* **2010**, *6*, 625–631.
- (26) Eggers, J. Nonlinear dynamics and breakup of free-surface flows. *Rev. Mod. Phys.* **1997**, *69*, 865–929.
- (27) Eggers, J.; Fontelos, M. A. *Singularities: Formation, Structure, and Propagation*; Cambridge University Press: Cambridge, UK, 2015; Vol. 53.
- (28) Basaran, O. A.; Gao, H.; Bhat, P. P. Nonstandard inkjets. *Annu. Rev. Fluid Mech.* **2013**, *45*, 85–113.
- (29) Basaran, O. A. Small-scale free surface flows with breakup: Drop formation and emerging applications. *AIChE J.* **2002**, *48*, 1842–1848.
- (30) Graham, M. D. Interfacial hoop stress and instability of viscoelastic free surface flows. *Phys. Fluids* **2003**, *15*, 1702.
- (31) Macosko, C. W. *Rheology: Principles, Measurements and Applications*; VCH Publishers Inc: New York, 1994.

- (32) James, D. F.; Walters, K. A critical appraisal of available methods for the measurement of extensional properties of mobile systems. In *Techniques of Rheological Measurement*; Collyer, A. A., Ed.; Elsevier: New York, 1994; pp 33–53.
- (33) Nguyen, T. Q.; Kausch, H. H. *Flexible Polymer Chains in Elongational Flow: Theory and Experiment*; Springer-Verlag: Berlin, 1999.
- (34) Miller, E.; Clasen, C.; Rothstein, J. P. The effect of step-stretch parameters on capillary breakup extensional rheology (CaBER) measurements. *Rheol. Acta* **2009**, *48*, 625–639.
- (35) Plog, J. P.; Kulicke, W. M.; Clasen, C. Influence of the molar mass distribution on the elongational behaviour of polymer solutions in capillary breakup. *Appl. Rheol.* **2005**, *15*, 28–37.
- (36) Vadodaria, S. S.; English, R. J. Extensional rheometry of cellulose ether solutions: flow instability. *Cellulose* **2016**, *23*, 339–355.
- (37) Christanti, Y.; Walker, L. M. Surface tension driven jet break up of strain-hardening polymer solutions. *J. Non-Newtonian Fluid Mech.* **2001**, *100*, 9–26.
- (38) Clasen, C.; Plog, J. P.; Kulicke, W. M.; Owens, M.; Macosko, C.; Scriven, L. E.; Verani, M.; McKinley, G. H. How dilute are dilute solutions in extensional flows? *J. Rheol.* **2006**, *50*, 849–881.
- (39) Bazilevsky, A. V.; Entov, V. M.; Rozhkov, A. N. Liquid Filament Microrheometer and Some of Its Applications. In *Third European Rheology Conference and Golden Jubilee Meeting of the British Society of Rheology*; Elsevier: Edinburgh, UK, 1990; pp 41–43.
- (40) Stelzer, M.; Brenn, G.; Yarin, A. L.; Singh, R. P.; Durst, F. Validation and application of a novel elongational device for polymer solutions. *J. Rheol.* **2000**, *44*, 595–616.
- (41) Bazilevskii, A. V.; Entov, V. M.; Rozhkov, A. N. Breakup of an Oldroyd liquid bridge as a method for testing the rheological properties of polymer solutions. *Polym. Sci., Ser. A* **2001**, *43*, 716–726.
- (42) Anna, S. L.; McKinley, G. H. Elasto-capillary thinning and breakup of model elastic liquids. *J. Rheol.* **2001**, *45*, 115–138.
- (43) Stelzer, M.; Brenn, G.; Yarin, A. L.; Singh, R. P.; Durst, F. Investigation of the elongational behavior of polymer solutions by means of an elongational rheometer. *J. Rheol.* **2002**, *46*, 507–527.
- (44) Bazilevsky, A. V.; Entov, V. M.; Rozhkov, A. N. Breakup of a liquid bridge as a method of rheological testing of biological fluids. *Fluid Dyn.* **2011**, *46*, 613–622.
- (45) Dinic, J.; Zhang, Y.; Jimenez, L. N.; Sharma, V. Extensional relaxation times of dilute, aqueous polymer solutions. *ACS Macro Lett.* **2015**, *4*, 804–808.
- (46) Dinic, J.; Biagioli, M.; Sharma, V. Pinch-off dynamics and extensional relaxation times of intrinsically semi-dilute polymer solutions characterized by dripping-onto-substrate rheometry. *J. Polym. Sci., Part B: Polym. Phys.* **2017**, *55*, 1692–1704.
- (47) Dinic, J.; Jimenez, L. N.; Sharma, V. Pinch-off dynamics and dripping-onto-substrate (DoS) rheometry of complex fluids. *Lab Chip* **2017**, *17*, 460–473.
- (48) Jimenez, L. N.; Dinic, J.; Parsi, N.; Sharma, V. Extensional relaxation time, pinch-off dynamics and printability of semi-dilute polyelectrolyte solutions. *Macromolecules* **2018**, *51*, 5191–5208.
- (49) Dinic, J.; Sharma, V. Macromolecular relaxation, strain, and extensibility determine elastocapillary thinning and extensional viscosity of polymer solutions. *Proc. Natl. Acad. Sci. U.S.A.* **2019**, *116*, 8766–8774.
- (50) Entov, V. M.; Hinch, E. J. Effect of a spectrum of relaxation times on the capillary thinning of a filament of elastic liquid. *J. Non-Newtonian Fluid Mech.* **1997**, *72*, 31–54.
- (51) Entov, V. M.; Yarin, A. L. Influence of elastic stresses on the capillary breakup of jets of dilute polymer solutions. *Fluid Dyn.* **1984**, *19*, 21–29.
- (52) Ardekani, A.; Sharma, V.; McKinley, G. H. Dynamics of bead formation, filament thinning and breakup of weakly viscoelastic jets. *J. Fluid Mech.* **2010**, *665*, 46–56.
- (53) Wagner, C.; Bourouiba, L.; McKinley, G. H. An analytic solution for capillary thinning and breakup of FENE-P fluids. *J. Non-Newtonian Fluid Mech.* **2015**, *218*, 53–61.
- (54) Prabhakar, R.; Gadkari, S.; Gopesh, T.; Shaw, M. J. Influence of stretching induced self-concentration and self-dilution on coil-stretch hysteresis and capillary thinning of unentangled polymer solutions. *J. Rheol.* **2016**, *60*, 345–366.
- (55) Prabhakar, R.; Sasmal, C.; Nguyen, D. A.; Sridhar, T.; Prakash, J. R. Effect of stretching-induced changes in hydrodynamic screening on coil-stretch hysteresis of unentangled polymer solutions. *Phys. Rev. Fluids* **2017**, *2*, No. 011301.
- (56) Zhou, J.; Doi, M. Dynamics of viscoelastic filaments based on Onsager principle. *Phys. Rev. Fluids* **2018**, *3*, No. 084004.
- (57) Tirtaatmadja, V.; McKinley, G. H.; Cooper-White, J. J. Drop formation and breakup of low viscosity elastic fluids: Effects of molecular weight and concentration. *Phys. Fluids* **2006**, *18*, No. 043101.
- (58) Sharma, V.; Ardekani, A. M.; McKinley, G. H. In 'Beads on a String' Structures and Extensional Rheometry using Jet Break-up, 5th Pacific Rim Conference on Rheology (PRCR-5), Sapporo, Japan, 2010.
- (59) Mathues, W.; Formenti, S.; McIlroy, C.; Harlen, O. G.; Clasen, C. CaBER vs ROJER-Different time scales for the thinning of a weakly elastic jet. *J. Rheol.* **2018**, *62*, 1135–1153.
- (60) Vadillo, D. C.; Mathues, W.; Clasen, C. Microsecond relaxation processes in shear and extensional flows of weakly elastic polymer solutions. *Rheol. Acta* **2012**, *51*, 755–769.
- (61) Arnolds, O.; Buggisch, H.; Sachsenheimer, D.; Willenbacher, N. Capillary breakup extensional rheometry (CaBER) on semi-dilute and concentrated polyethyleneoxide (PEO) solutions. *Rheol. Acta* **2010**, *49*, 1207–1217.
- (62) Rodd, L. E.; Scott, T. P.; Cooper-White, J. J.; McKinley, G. H. Capillary break-up rheometry of low-viscosity elastic fluids. *Appl. Rheol.* **2005**, *15*, 12–27.
- (63) Sachsenheimer, D.; Hochstein, B.; Willenbacher, N. Experimental study on the capillary thinning of entangled polymer solutions. *Rheol. Acta* **2014**, *53*, 725–739.
- (64) Campo-Deaño, L.; Clasen, C. The slow retraction method (SRM) for the determination of ultra-short relaxation times in capillary breakup extensional rheometry experiments. *J. Non-Newtonian Fluid Mech.* **2010**, *165*, 1688–1699.
- (65) Wunderlich, T.; Stelzer, M.; Tripathy, T.; Nayak, B. R.; Brenn, G.; Yarin, A. L.; Singh, R. P.; Brunn, P. O.; Durst, F. Shear and extensional rheological investigations in solutions of grafted and ungrafted polysaccharides. *J. Appl. Polym. Sci.* **2000**, *77*, 3200–3209.
- (66) Szopinski, D.; Handge, U. A.; Kulicke, W.-M.; Abetz, V.; Luinstra, G. A. Extensional flow behavior of aqueous guar gum derivative solutions by capillary breakup elongational rheometry (CaBER). *Carbohydr. Polym.* **2016**, *136*, 834–840.
- (67) Bingöl, A. Ö.; Lohmann, D.; Püschel, K.; Kulicke, W.-M. Characterization and comparison of shear and extensional flow of sodium hyaluronate and human synovial fluid. *Biorheology* **2010**, *47*, 205–224.
- (68) Storz, H.; Zimmermann, U.; Zimmermann, H.; Kulicke, W.-M. Viscoelastic properties of ultra-high viscosity alginates. *Rheol. Acta* **2010**, *49*, 155–167.
- (69) De Dier, R.; Mathues, W.; Clasen, C. Extensional flow and relaxation of semi-dilute solutions of schizophyllan. *Macromol. Mater. Eng.* **2013**, *298*, 944–953.
- (70) Rodríguez-Rivero, C.; Hilliou, L.; del Valle, E. M. M.; Galán, M. A. Rheological characterization of commercial highly viscous alginate solutions in shear and extensional flows. *Rheol. Acta* **2014**, *53*, 559–570.
- (71) Naik, S. C.; Pittman, J. F. T.; Richardson, J. F. The rheology of hydroxyethyl cellulose solutions. *Trans. Soc. Rheol.* **1976**, *20*, 639–649.
- (72) Tanaka, R.; Meadows, J.; Phillips, G. O.; Williams, P. A. Viscometric and spectroscopic studies on the solution behavior of hydrophobically modified cellulose polymers. *Carbohydr. Polym.* **1990**, *12*, 443–459.

- (73) Meadows, J.; Williams, P. A.; Kennedy, J. C. Comparison of the extensional and shear viscosity characteristics of aqueous hydroxyethyl cellulose solutions. *Macromolecules* **1995**, *28*, 2683–2692.
- (74) Maestro, A.; Gonzalez, C.; Gutierrez, J. M. Shear thinning and thixotropy of HMHEC and HEC water solutions. *J. Rheol.* **2002**, *46*, 1445–1457.
- (75) Patruyo, L. G.; Muller, A. J.; Saez, A. E. Shear and extensional rheology of solutions of modified hydroxyethyl celluloses and sodium dodecyl sulfate. *Polymer* **2002**, *43*, 6481–6493.
- (76) Laschet, M.; Plog, J. P.; Clasen, C.; Kulicke, W.-M. Examination of the flow behaviour of HEC and hmHEC solutions using structure–property relationships and rheo-optical methods. *Colloid Polym. Sci.* **2004**, *282*, 373–380.
- (77) Maestro, A.; Gonzalez, C.; Gutierrez, J. M. Rheological behavior of hydrophobically modified hydroxyethyl cellulose solutions: A linear viscoelastic model. *J. Rheol.* **2002**, *46*, 127–143.
- (78) González, J. M.; Müller, A. J.; Torres, M. F.; Saez, A. E. The role of shear and elongation in the flow of solutions of semi-flexible polymers through porous media. *Rheol. Acta* **2005**, *44*, 396–405.
- (79) Arfin, N.; Bohidar, H. B. Concentration selective hydration and phase states of hydroxyethyl cellulose (HEC) in aqueous solutions. *Int. J. Biol. Macromol.* **2012**, *50*, 759–767.
- (80) Vadodaria, S. S.; English, R. J. Aqueous solutions of HEC and hmHEC: effects of molecular mass versus hydrophobic associations on hydrodynamic and thermodynamic parameters. *Cellulose* **2016**, *23*, 1107–1121.
- (81) Del Giudice, F.; Tassieri, M.; Oelschlaeger, C.; Shen, A. Q. When Microrheology, Bulk Rheology, and Microfluidics Meet: Broadband Rheology of Hydroxyethyl Cellulose Water Solutions. *Macromolecules* **2017**, *50*, 2951–2963.
- (82) Doshi, P.; Suryo, R.; Yildirim, O. E.; McKinley, G. H.; Basaran, O. A. Scaling in pinch-off of generalized Newtonian fluids. *J. Non-Newtonian Fluid Mech.* **2003**, *113*, 1–27.
- (83) Doshi, P.; Basaran, O. A. Self-similar pinch-off of power law fluids. *Phys. Fluids* **2004**, *16*, S85–S93.
- (84) Suryo, R.; Basaran, O. A. Local dynamics during pinch-off of liquid threads of power law fluids: Scaling analysis and self-similarity. *J. Non-Newtonian Fluid Mech.* **2006**, *138*, 134–160.
- (85) Niedzwiedz, K.; Buggisch, H.; Willenbacher, N. Extensional rheology of concentrated emulsions as probed by capillary breakup elongational rheometry (CaBER). *Rheol. Acta* **2010**, *49*, 1103–1116.
- (86) Huisman, F. M.; Friedman, S. R.; Taborek, P. Pinch-off dynamics in foams, emulsions and suspensions. *Soft Matter* **2012**, *8*, 6767–6774.
- (87) Zhang, Y.; Muller, S. J. Unsteady sedimentation of a sphere in wormlike micellar fluids. *Phys. Rev. Fluids* **2018**, *3*, No. 043301.
- (88) Schneider, C. A.; Rasband, W. S.; Eliceiri, K. W. NIH Image to ImageJ: 25 years of image analysis. *Nat. Methods* **2012**, *9*, 671–675.
- (89) Hsiao, K. W.; Dinic, J.; Ren, Y.; Sharma, V.; Schroeder, C. M. Passive non-linear microrheology for determining extensional viscosity. *Phys. Fluids* **2017**, *29*, No. 121603.
- (90) Walter, A. V.; Jimenez, L. N.; Dinic, J.; Sharma, V.; Erk, K. A. Effect of salt valency and concentration on shear and extensional rheology of aqueous polyelectrolyte solutions for enhanced oil recovery. *Rheol. Acta* **2019**, *58*, 145–157.
- (91) Marshall, K. A.; Liedtke, A. M.; Todt, A. H.; Walker, T. W. Extensional rheometry with a handheld mobile device. *Exp. Fluids* **2017**, *58*, No. 69.
- (92) Suteria, N. S.; Gupta, S.; Potineni, R.; Baier, S. K.; Vanapalli, S. A. eCapillary: a disposable microfluidic extensional viscometer for weakly elastic polymeric fluids. *Rheol. Acta* **2019**, *58*, 403–417.
- (93) Marshall, K. A.; Walker, T. W. Investigating the dynamics of droplet breakup in a microfluidic cross-slot device for characterizing the extensional properties of weakly-viscoelastic fluids. *Rheol. Acta* **2019**, *58*, 573–590.
- (94) Pack, M. Y.; Yang, A.; Perazzo, A.; Qin, B.; Stone, H. A. Role of extensional rheology on droplet bouncing. *Phys. Rev. Fluids* **2019**, *4*, No. 123603.
- (95) Rosello, M.; Sur, S.; Barbet, B.; Rothstein, J. P. Dripping-onto-substrate capillary breakup extensional rheometry of low-viscosity printing inks. *J. Non-Newtonian Fluid Mech.* **2019**, *266*, 160–170.
- (96) Wu, S. J.; Mohammadigoushki, H. Sphere sedimentation in wormlike micelles: Effect of micellar relaxation spectrum and gradients in micellar extensions. *J. Rheol.* **2018**, *62*, 1061–1069.
- (97) Omidvar, R.; Wu, S.; Mohammadigoushki, H. Detecting wormlike micellar microstructure using extensional rheology. *J. Rheol.* **2019**, *63*, 33–44.
- (98) Cross, M. M. Rheology of non-Newtonian fluids - A new flow equation for pseudoplastic systems. *J. Colloid Sci.* **1965**, *20*, 417–437.
- (99) Morris, E. R.; Cutler, A. N.; Ross-Murphy, S. B.; Rees, D. A.; Price, J. Concentration and shear rate dependence of viscosity in random coil polysaccharide solutions. *Carbohydr. Polym.* **1981**, *1*, 5–21.
- (100) Morris, E. R. Shear thinning of random coil polysaccharides: Characterization by two parameters from a simple linear plot. *Carbohydr. Polym.* **1990**, *13*, 85–96.
- (101) Doi, M.; Edwards, S. F. *The Theory of Polymer Dynamics*; Oxford University Press: New York, 1986; p 406.
- (102) Rubinstein, M.; Colby, R. H. *Polymer Physics*; Oxford Univ. Press: New York, 2003.
- (103) Larson, R. G. The rheology of dilute solutions of flexible polymers: Progress and problems. *J. Rheol.* **2005**, *49*, 1–70.
- (104) Couvelier, G.; Launay, B. Concentration regimes in xanthan gum solutions deduced from flow and viscoelastic properties. *Carbohydr. Polym.* **1986**, *6*, 321–333.
- (105) Haward, S. J.; Sharma, V.; Butts, C. P.; McKinley, G. H.; Rahatekar, S. S. Shear and extensional rheology of cellulose/ionic liquid solutions. *Biomacromolecules* **2012**, *13*, 1688–1699.
- (106) Morse, D. C. Viscoelasticity of tightly entangled solutions of semiflexible polymers. *Phys. Rev. E* **1998**, *58*, R1237–R1240.
- (107) Morse, D. C. Viscoelasticity of concentrated isotropic solutions of semiflexible polymers. 1. Model and stress tensor. *Macromolecules* **1998**, *31*, 7030–7043.
- (108) Morse, D. C. Viscoelasticity of concentrated isotropic solutions of semiflexible polymers. 2. Linear response. *Macromolecules* **1998**, *31*, 7044–7067.
- (109) Broedersz, C. P.; MacKintosh, F. C. Modeling semiflexible polymer networks. *Rev. Mod. Phys.* **2014**, *86*, 995.
- (110) Koenderink, G. H.; Atakhorrami, M.; MacKintosh, F. C.; Schmidt, C. F. High-frequency stress relaxation in semiflexible polymer solutions and networks. *Phys. Rev. Lett.* **2006**, *96*, No. 138307.
- (111) Lang, C.; Hendricks, J.; Zhang, Z.; Reddy, N. K.; Rothstein, J. P.; Lettinga, M. P.; Vermant, J.; Clasen, C. Effects of particle stiffness on the extensional rheology of model rod-like nanoparticle suspensions. *Soft Matter* **2019**, *15*, 833–841.
- (112) Rayleigh, L. On the capillary phenomenon of jets. *Proc. R. Soc. London* **1879**, *29*, 71–97.
- (113) Middleman, S. *Modeling Axisymmetric Flows: Dynamics of Films, Jets and Drops*; Academic Press: San Diego, 1995.
- (114) Chen, Y.-J.; Steen, P. Dynamics of inviscid capillary breakup: collapse and pinchoff of a film bridge. *J. Fluid Mech.* **1997**, *341*, 245–267.
- (115) Day, R. F.; Hinch, E. J.; Lister, J. R. Self-similar capillary pinchoff of an inviscid fluid. *Phys. Rev. Lett.* **1998**, *80*, 704–707.
- (116) Dinic, J.; Sharma, V. Computational analysis of self-similar capillary-driven thinning and pinch-off dynamics during dripping using the Volume-of-Fluid method. *Phys. Fluids* **2018**, *31*, No. 021211.
- (117) Deblais, A.; Herrada, M. A.; Hauner, I.; Velikov, K. P.; Van Roon, T.; Kellay, H.; Eggers, J.; Bonn, D. Viscous Effects on Inertial Drop Formation. *Phys. Rev. Lett.* **2018**, *121*, No. 254501.
- (118) Papageorgiou, D. T. On the breakup of viscous liquid threads. *Phys. Fluids* **1995**, *7*, 1529–1544.
- (119) Fontelos, M. A.; Li, J. On the evolution and rupture of filaments in Giesekus and FENE models. *J. Non-Newtonian Fluid Mech.* **2004**, *118*, 1–16.

- (120) Wagner, C.; Amarouchene, Y.; Bonn, D.; Eggers, J. Droplet detachment and satellite bead formation in viscoelastic fluids. *Phys. Rev. Lett.* **2005**, *95*, No. 164504.
- (121) Amarouchene, Y.; Bonn, D.; Meunier, J.; Kellay, H. Inhibition of the finite-time singularity during droplet fission of a polymeric fluid. *Phys. Rev. Lett.* **2001**, *86*, 3558–3561.
- (122) Zell, A.; Gier, S.; Rafai, S.; Wagner, C. Is there a Relationship between the Elongational Viscosity and the First Normal Stress Difference in Polymer Solutions? *J. Non-Newtonian Fluid Mech.* **2010**, *165*, 1265–1274.
- (123) Sattler, R.; Gier, S.; Eggers, J.; Wagner, C. The final stages of capillary break-up of polymer solutions. *Phys. Fluids* **2012**, *24*, No. 023101.
- (124) Gaume, L.; Forterre, Y. A viscoelastic deadly fluid in carnivorous pitcher plants. *PLoS One* **2007**, *2*, No. e1185.
- (125) Erni, P.; Varagnat, M.; Clasen, C.; Crest, J.; McKinley, G. H. Microrheometry of sub-nanolitre biopolymer samples: non-Newtonian flow phenomena of carnivorous plant mucilage. *Soft Matter* **2011**, *7*, 10889–10898.
- (126) Collett, C.; Ardron, A.; Bauer, U.; Chapman, G.; Chaudan, E.; Hallmark, B.; Pratt, L.; Torres-Perez, M. D.; Wilson, D. I. A portable extensional rheometer for measuring the viscoelasticity of pitcher plant and other sticky liquids in the field. *Plant Methods* **2015**, *11*, 16.
- (127) Oliveira, M. S. N.; Yeh, R.; McKinley, G. H. Iterated stretching, extensional rheology and formation of beads-on-a-string structures in polymer solutions. *J. Non-Newtonian Fluid Mech.* **2006**, *137*, 137–148.
- (128) Oliveira, M. S. N.; McKinley, G. H. Iterated stretching and multiple beads-on-a-string phenomena in dilute solutions of highly extensible flexible polymers. *Phys. Fluids* **2005**, *17*, No. 071704.
- (129) Nelson, W. C.; Kavehpour, H. P.; Kim, C. J. A miniature capillary breakup extensional rheometer by electrostatically assisted generation of liquid filaments. *Lab Chip* **2011**, *11*, 2424–2431.
- (130) Jaishankar, A.; Wee, M.; Matia-Merino, L.; Goh, K. K. T.; McKinley, G. H. Probing hydrogen bond interactions in a shear thickening polysaccharide using nonlinear shear and extensional rheology. *Carbohydr. Polym.* **2015**, *123*, 136–145.
- (131) Bhardwaj, A.; Miller, E.; Rothstein, J. P. Filament stretching and capillary breakup extensional rheometry measurements of viscoelastic wormlike micelle solutions. *J. Rheol.* **2007**, *51*, 693–719.
- (132) Chellamuthu, M.; Rothstein, J. R. Distinguishing between linear and branched wormlike micelle solutions using extensional rheology measurements. *J. Rheol.* **2008**, *52*, 865–884.
- (133) Bhardwaj, A.; Richter, D.; Chellamuthu, M.; Rothstein, J. P. The effect of pre-shear on the extensional rheology of wormlike micelle solutions. *Rheol. Acta* **2007**, *46*, 861–875.
- (134) Hussainov, M.; Tätte, T.; Hussainova, I. Technique for extensional rheology characterization of highly reactive viscoelastic liquids. *Rheol. Acta* **2012**, *51*, 729–742.
- (135) Khandavalli, S.; Rothstein, J. P. Extensional rheology of shear-thickening fumed silica nanoparticles dispersed in an aqueous polyethylene oxide solution. *J. Rheol.* **2014**, *58*, 411–431.
- (136) Clasen, C. Capillary breakup extensional rheometry of semi-dilute polymer solutions. *Korea-Australia Rheol. J.* **2010**, *22*, 331–338.
- (137) Fujii, S.; Sasaki, N.; Nakata, M. Phenomenological analysis of elongational flow birefringence in semidilute solutions of hydroxypropylcellulose. *Colloid Polym. Sci.* **2003**, *281*, 823–831.
- (138) Eley, R. R. Applied rheology in the protective and decorative coatings industry. *Rheol. Rev.* **2005**, 173–240.
- (139) Chatterjee, T.; Nakatani, A. I.; Van Dyk, A. K. Shear-Dependent Interactions in Hydrophobically Modified Ethylene Oxide Urethane (HEUR) Based Rheology Modifier–Latex Suspensions: Part 1. Molecular Microstructure. *Macromolecules* **2014**, *47*, 1155–1174.
- (140) Van Dyk, A. K.; Chatterjee, T.; Ginzburg, V. V.; Nakatani, A. I. Shear-Dependent Interactions in Hydrophobically Modified Ethylene Oxide Urethane (HEUR) Based Coatings: Mesoscale Structure and Viscosity. *Macromolecules* **2015**, *48*, 1866–1882.
- (141) Shaqfeh, E. S. G. On the rheology of particle suspensions in viscoelastic fluids. *AIChE J.* **2019**, *65*, No. e16575.